The Influence of pH and Electrolyte Concentration on Fractional Protonation and CO_2 Reduction Activity in Polymer-Encapsulated Cobalt Phthalocyanine

Taylor L. Soucy,[1] *William S. Dean,* [1] *Kevin E. Rivera Cruz,* [1] *Jonah B. Eisenberg,* [1] *Lirong Shi,*[1] *Charles C. L. McCrory* [1,2*]

[1] Chemistry Department, University of Michigan, 930 N. University Ave. Ann Arbor, MI, 48109, United States.

[2] Macromolecular Sciences and Engineering Program, University of Michigan, 930 N. University Ave. Ann Arbor, MI, 48109, United States.

ABSTRACT

Polymer-encapsulated cobalt phthalocyanine (CoPc) is a model system for studying how polymer-catalyst interactions in the electrocatalytic systems influence performance for the CO_2 reduction reaction. In particular, understanding how bulk electrolyte and proton concentration influences polymer protonation, and in turn how the extent of polymer protonation influences catalytic activity and selectivity, is crucial to understanding polymer-catalyst composite materials.

We report a study of the dependence of bulk pH and electrolyte concentration on the fractional protonation of poly-4-vinylpyridine and related polymers with both electrochemical and spectroscopic evidence. In addition, we show that the fractional protonation of the polymer is directly related to both the activity of the catalyst and the reaction selectivity for the CO_2 reduction reaction over the competitive hydrogen evolution reaction. Of particular note is that the fractional protonation of the film is related to electrolyte concentration, which suggests that the transport of counterions plays an important role in regulating proton transport within the polymer film. These insights suggest that electrolyte concentration and pH play an important in the electrocatalytic performance for polymer-catalyst composite systems, and these influences should be considered in both experimental preparation and analysis.

INTRODUCTION

The conversion of industrial waste CO_2 into value-added products using renewable energy is one proposed way to harness intermittent energy sources while decreasing net CO_2 emissions.[1-11] In particular, the electrochemical CO_2 reduction reaction (CO_2RR) is an important strategy for CO_2 conversion, but requires the development of electrocatalytic systems incorporating molecular[12-17] or solid-state catalysts[18-24] to drive the kinetically-demanding reactions. Regardless of catalyst system chosen, a major barrier to practical CO_2 reduction is reaction and product selectivity, especially outcompeting the competitive hydrogen evolution reaction (HER).[25-27]

Porphyrins and phthalocyanines have been studied as molecular electrocatalysts for the CO_2RR, with cobalt phthalocyanine (CoPc) being a particularly well-studied catalyst due to its unique electron configuration and favorable binding energy to CO_2.[28-41] CoPc easily adsorbs to carbon electrode surfaces and has been an important model system to study the mechanism of the

CO_2RR,[40,41] as well as one of the rare molecular catalysts able to reduce CO_2 to methanol under specific reaction conditions.[28,38] Our particular interest in CoPc has focused on improving the selectivity of CoPc-catalyzed CO_2RR over the competing HER by encapsulating the parent complex within coordinating polymers to control the local microenvironment. Our group[42] and others[43,44] have shown that encapsulating CoPc within poly(4-vinylpyridine) (P4VP) results in increased reaction activity and selectivity for the CO_2RR over the HER, leading to an increase in Faradaic efficiency for CO production from 60% for CoPc to > 90% for CoPc-P4VP and a four-fold increase in turnover frequency for CO production.[37,42,45]

Previous studies within our group have focused on understanding the role of the encapsulating P4VP polymer in modulating the primary, secondary, and outer coordination sphere surrounding the CoPc catalyst, and how changes to these coordination spheres influence activity and reaction selectivity for the CO_2RR.[37,42,45-49] In particular, we provided experimental evidence through kinetic isotope effect and proton inventory studies to show that the pyridyl residues in the P4VP polymer are crucial for controlling proton transport through the polymer to the catalyst active sites, and that this proton transport within the polymer-catalyst system likely occurs via a multi-site proton relay mechanism rather than diffusion-controlled transport.[37]

A complicating factor for polymer-encapsulated catalyst systems is that the protonated pyridyl residues likely not only serve as a multisite proton relay, but also provide local buffering near the catalyst sites. The pKa of protonated pyridyl residues within P4VP is 3.5, slightly lower than the analogous monomer due to the hydrophobic backbone of the polymer.[50] An outstanding research question in polymer-catalyst composites with such proton relays is how the bulk electrolyte pH affects the transport and buffering of H^+ within the polymer, and what effect this transport and buffering has on the catalytic activity. Numerous studies have indicated that pH is important in

practical applications for the reduction of CO_2 in an electrochemical fuel cell system, especially when considering the impact of electrolyte identity and concentration on local pH in polymer-catalyst composites.[51-53] Considering most practical catalysts for the CO_2RR employ a polymer binder to adhere the catalyst to the electrode surface, we believe that understanding how bulk pH affects catalyst performance for the CoPc-P4VP model system will provide important insights in understanding these effects in these other polymer-catalyst composite materials.

In this work, we quantitatively measure the impact of changes to bulk pH and electrolyte concentration on the fractional protonation of the P4VP in CoPc-P4VP composite materials, and we determine the impact these changes in fractional protonation have on the catalytic activity and selectivity for CO_2 reduction. We use *ex situ* infrared spectroscopy to characterize the fractional protonation of the P4VP polymer in the CoPc-P4VP system, and we correlate this fractional protonation with observed changes in electrocatalytic activity. We hypothesized that at intermediate bulk pH ~5, the P4VP polymer would be only partially protonated, allowing proton transport via a multisite proton relay (Figure 1). Under more acidic bulk conditions (pH ~3), we hypothesized that the polymer is fully protonated and therefore proton delivery is rapid to the catalyst site. Under such conditions, we postulated that the overall catalytic current density would be higher, but a larger fraction of this current density would be going towards competitive HER compared to the CoPc-P4VP system at bulk pH 5, leading to an overall decrease in fractional current density going to CO (j_{CO}). In contrast, at bulk pH 7, we hypothesized that the polymer would be fully deprotonated, leading to diffusional control of H^+ transport in the polymer. We postulated that this lower rate of H^+ transport at bulk pH 7 should lead to higher reaction selectivity for the CO_2RR over competitive HER, but lower overall activity. Overall, we expected the CoPc-P4VP system to achieve the maximum activity for the CO_2RR at intermediate pH ~5 (Figure 1).

Our experimental results largely confirm these hypotheses, with a few caveats. In addition, we show that the extent of fractional protonation is also governed by the electrolyte concentration, leading to an increase in activity but a decrease in selectivity for the CO_2RR. This suggests that the partitioning of protons within the encapsulating polymer is not only dependent on the bulk pH, but also on the concentration of the buffering anions in solution. These studies provide important insights into how choices of pH, electrolyte identity, and electrolyte concentration can influence electrocatalytic activity for small-molecule transformations in polymer-catalyst composite materials.

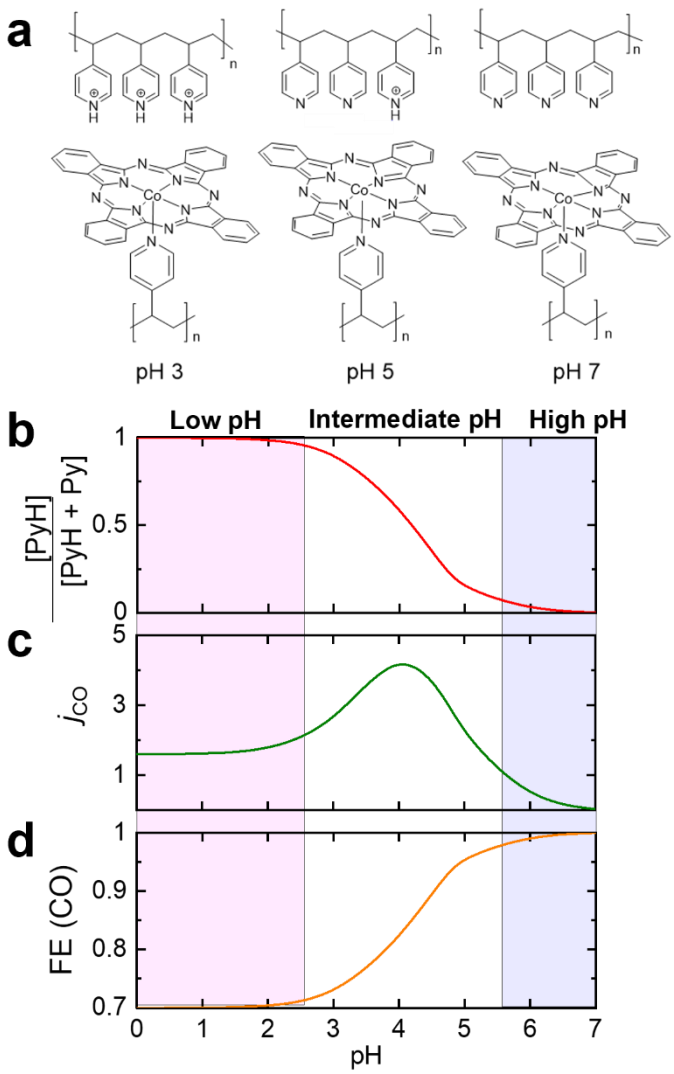

Figure 1. (a) Schematic representation of the postulated extent of fractional protonation of the polymer pyridyl moieties in CoPc-P4VP as a function of bulk pH, expanded on graphically in (b), where fractional protonation decreases as bulk electrolyte pH increases due to the decrease in available protons. (c) The hypothesized change in partial current density for CO production (j_{CO}), a measure of activity for the CO_2RR, as a function of bulk pH. At low bulk pH, we postulate that competitive HER will be the dominant reaction in the CoPc-P4VP system due to the high availability of protonated pyridyl moieties, leading to comparatively low activity for the CO_2RR. At high bulk pH, we postulate that the CO_2RR activity will be limited by reduced availability of protons due to the full deprotonation of the pyridyl moieties within CoPc-P4VP. The highest activity is hypothesized at intermediate pH ~5, where the CO_2RR is the dominant reaction but there is a reasonable availability of protons within the CoPc-P4VP polymer

composite. (d) The hypothesized changes in Faradaic efficiency (FE(CO)) for CO production as a function of bulk pH. We postulate that increasing the bulk pH will increase the reaction selectivity for CO_2RR by limiting the availability of protons within the CoPc-P4VP system for the competitive HER.

EXPERIMENTAL

Materials

All purchased chemicals were used as received, unless otherwise specified. All water used in this study was ultrapure water (18.2 MΩ cm resistivity), prepared via purification by a Thermo Scientific GenPure UV-TOC/UF x CAD-plus water purification system. Carbon dioxide (CO_2, 99.8%) was purchased from Cryogenic Gases and was used as received, and nitrogen (N_2) was boil-off gas from a liquid nitrogen source and was used without further purification. The following chemicals were purchased from Sigma Aldrich and used as received: graphite powder (GP, synthetic < 20 μm), cobalt phthalocyanine (CoPc, 97%), poly-4-vinylpyridine (P4VP, average Mw ~ 160,000), N, N-Dimethylformamide (DMF, ACS grade), poly-2-vinylpyridine (P2VP, average Mw ~159,000), sodium phosphate monobasic (NaH_2PO_4, BioXtra, >99.0%), phosphoric acid (85 wt% in H_2O), Nafion-117 cation exchange membrane (Nafion), ferrocene carboxylic acid (97%), and sodium hydroxide (NaOH, TraceMetal grade). Sodium perchlorate monohydrate ($NaClO_4 \cdot H_2O$, 97%) was obtained from Alfa Aesar. Nitric acid (TraceMetal grade, 67-70%) was purchased from Fisher Scientific. Cobalt ICP standard (1000 ppm in 3% HNO_3) was purchased from Ricca Chemical Company. Glassy carbon disk electrodes (GCEs, 4 mm thick, 5 mm in diameter, effective electrode area 0.196 cm^2) were purchased from HTW Hochtemperatur-Werkstoff GmbH.

Electrolyte Solution Preparation and pH Measurements

Unless otherwise stated, all experiments were performed in phosphate/perchlorate electrolyte solutions with concentrations explicitly stated in the main text and captions. Experiments performed to determine the pH dependence of the electrochemical system were performed in electrolyte solutions of 0.4 M NaH_2PO_4 added to 0.5 M $NaClO_4$. The use of $NaClO_4$ was used to maintain close to the same ionic strength regardless of solution pH. Experiments used to study the activity dependence of electrolyte concentration were performed in varying concentrations of phosphate/perchlorate buffer systems as specified in the main text, including the systems where there was only phosphate and no perchlorate in the electrolyte. Importantly, all electrochemical glassware were vigorously washed between experiments, all electrochemical cells and Nafion membrane separators were soaked in ultrapure water for at least 12 hours prior to use to ensure that all electrolyte salts were removed.

It would be challenging to determine the exact speciation of ions in our solution, and therefore the exact ionic strength, given the complexity of the electrolyte containing ions from a mixture of pH-dependent $H_3PO_4/H_2PO_4^-/HPO_4^{2-}$ and CO_2/HCO_3^- buffers. However, although we are unable to measure the quantitative ionic strength, we are able to predict qualitative changes in ionic strength from systematic modifications of the electrolyte by considering three core assumptions: (1) The effects of ion concentration on buffer ion activity, and therefore pKa, are small in the concentration range of interest (~0.1 M to 1.0 M total ion concentration). For example, the pKa of phosphate changes from ~6.81 in 0.1 M electrolyte, to ~6.67 in 0.4 M electrolyte, to ~6.62 in 1.0 M electrolyte.[54] (2) The concentration of $H_2PO_4^-$ and HPO_4^{2-} do not change appreciably between $6 \geq pH \geq 4$. Because this pH range is far from the $H_2PO_4^-/HPO_4^{2-}$ pKa, the buffer is mostly composed of $H_2PO_4^-$, and relatively large changes in pH result in relatively small changes

in buffer ion concentrations. (3) The total amount of carbonate in solution due to CO_2 sparging is small compared to other ions in solution (<0.035 mol/L).[55] So although we are unable to measure quantitative changes in ionic strength in our studies, we are able to predict qualitative trends in ionic strength sufficiently well so that any small variations do not influence our data analysis and conclusions.

Prior to each experiment, the working chamber was sparged with the appropriate gas for at least 30 minutes. The pH after sparging varied from between 4.1 to 4.5 and was adjusted to the desired pH level for the experiment by titrating 1 M NaOH or 10% H_3PO_4 into the electrolyte while it was blanketed by CO_2 or N_2 and sealed under 1 atm of the appropriate gas. Note that all phosphate buffer concentrations reported are inclusive any added H_3PO_4 to +/- 0.01 M accuracy. All pH measurements were conducted with a Fisher Scientific Accumet AB200 pH meter with an Atlas Scientific pH probe calibrated at three points with pH = 4.01, 7.00, and 10.01 calibration standards (Fisher Scientific).

Preparation of Catalyst Deposition Inks (CoPc-P4VP/GP)

CoPc-polymer/GP deposition inks were prepared as previously described.[56] The preparation conditions and resultant loadings of catalyst, polymer, and graphite powder can be found in Supplementary Table S1. A solution of 0.05 mM CoPc in DMF was prepared by the addition of 0.0029 g of CoPc to 100 mL of DMF in a duct tape-jacketed 100 mL glass bottle. The duct tape jacketing mitigated the possibility of photodegradation of the CoPc during solution preparation. The mixture was sonicated for 1 hour and then vortexed for 1 minute at 3000 rpm. Following the preparation of the 0.05 mM CoPc/DMF solution, 0.03 g polymer was added to 1 mL of the CoPc/DMF mixture in a 20 mL duct tape-jacketed scintillation vial to create a 0.05 mM CoPc –

3% w/v polymer in DMF. The P4VP was allowed to disperse by sonication for 30 minutes. A mass of 0.01 g of graphite powder was then added to the CoPc-polymer mixture to create a 0.05 mM CoPc – 3% P4VP – 1% w/v GP preparation suspension. The suspension was allowed to disperse via sonication for 30 minutes. A Teflon stirbar was then added to the scintillation vial and the CoPc-polymer/GP mixture was magnetically stirred by stirplate at 500 rpm for 12 h. After stirring, the preparation suspension was centrifuged in a 2 mL centrifuge tube (Fisherbrand Premium Microcentrifuge tube) at 14,000 rpm for 30 minutes at −4 ºC in an Eppendorf 5430R refrigerated centrifuge. The supernatant was decanted, and 1 mL of fresh DMF was added. The suspension was then vortexed for 30 sec at 3000 rpm, and sonicated for 30 sec.

Preparation of Modified Electrodes (CoPc-P4VP/GP/GCE)

Prior to modification, glassy carbon electrodes (GCEs) were polished on a Struers LaboPol-5 polishing instrument with a LaboForce-1 specimen mover. The GCE disks were loaded into a custom-made brass electrode holder held by the specimen mover with polishing side pressed against a MDFloc (Struers) synthetic nap polishing pad. The GCE disks were sequentially polished with diamond abrasive slurries (DiaDuo-2, Struers) in an order of 9 µm, 6 µm, 3 µm, and 1 µm diameter particle slurries for 1 minute. The speed of the platen was held at 200 rpm and, and the specimen mover rotated at a speed of 8 pm in the opposite rotation direction from the platen. Between each polishing step, electrodes were rinsed with ultrapure water. After the final polishing step, the GCE disks were sonicated in isopropyl alcohol for 3 minutes, followed by ultrapure water for 3 minutes, and in 1 M HNO_3 for 30 minutes. The electrodes were then rinsed with ultrapure water and dried under an N_2 stream. All electrodes were dried in an oven at 60 ºC for 10 minutes immediately prior to the dropcasting of deposition ink. The electrodes were coated by dropcasting

5 µL of the CoPc-P4VP/GP deposition ink, allowing the surface to dry in an oven at 60ºC for 10 minutes, and then was followed by a second coating of 5 µL of the deposition ink and drying at the same temperature.

Cobalt Loading Determination

Catalyst loading was determined as previously described.[30] After centrifugation, the graphitic pellet was digested by the addition of 15 mL TraceMetal Grade 1 M HNO_3. The solution was stirred overnight, and then was filtered using a cellulose syringe (Pore Size 0.45 µm, Titan 3 regenerated cellulose, Fisher Scientific) to remove the polymer and graphite powder. The metal content was then measured using inductively coupled plasma-mass spectrometry (ICP-MS, PerkinElmer Nexion2000). The ICP-MS was calibrated using internal standards at 10, 50, 100, and 500 ppb and standard nitric acid blank at 0 ppb. The conversion from ppb to molar CoPc loading in the deposition ink is shown in Equations 1-3.

$$X \text{ ppb} \times \frac{\frac{1\ \mu g}{\text{L}}}{1 \text{ ppb}} \times 0.015 \text{ L} = \text{mass Co in } \mu\text{g} \quad (1)$$

$$\text{mass in } \mu\text{g x } \frac{1 \text{ mol Co}}{58.93 \text{ g Co}} \times \frac{10^{-6} \text{ g}}{1\ \mu\text{g}} = \text{ mol CoPc} \quad (2)$$

$$\frac{\text{mol CoPc}}{0.0010 \text{ L initial deposition ink}} = M \text{ CoPc in deposition ink} \quad (3)$$

Electrochemical Measurements

Electrochemical measurements were conducted using a Bio-Logic SP200 potentiostat/galvanostat, and data were recorded using the Bio-Logic EC-Lab software package. Reference electrodes were commercial saturated calomel electrode (SCE), externally referenced

to ferrocenecarboxylic acid in pH 7, 0.2 M phosphate buffer (0.284 V vs. SCE), and auxiliary electrodes were carbon rods (99.999%, Strem Chemicals Inc.). Working electrodes were the modified GCEs described in the previous section. The working electrode was separated from the auxiliary electrode by a Nafion membrane. Unless otherwise noted, all electrochemical measurements were conducted at least three times with independently prepared electrodes, all values reported are the average of these repetitions, and all reported errors are standard deviations. The reported errors of interpretations that required mathematical operations are reported as standard errors.

For rotating disk electrode (RDE) chronoamperomentric (CA) step measurements, the modified GCE working compartment was assembled using a Pine Research Instrumentation E6-series change disk RDE assembly attached to an MSR rotator. CA measurements were conducted at 1600 rotations per minute (rpm) with a single 6-minute potential step held at -0.647 V vs. RHE (V vs. SCE varied depending on the electrolyte pH), to ensure equivalent thermodynamic potential against the concentration of protons. The 1600 rpm rotation rate was used to ensure steady-state CO_2 and/or proton delivery to the electrode surface.

RDE-CA measurements were conducted in a previously reported custom two-compartment glass cell.[37] In the first compartment, the working electrode with GCE assembly was suspended in 30 mL buffer solution with 3 gas inlets and one inlet for the reference electrode. The second compartment contained ~15 mL solution with the auxiliary electrode. The compartments were separated by a Nafion membrane. Both compartments were sparged with the gas (CO_2 or N_2) for ~30 minutes prior to each set of measurements, and the headspace was blanketed with the corresponding gas during the measurements. The gas used for all electrochemical experiments was first saturated with electrolyte solvent by bubbling the gas through a gas washing bottle filled with

the same electrolyte solvent (water or deuterium oxide) used in the cell to minimize electrolyte evaporation in the cell during the course of the measurements. Solution resistance of the cell was measured prior to experiments using a single-point high frequency impedance measurement, and was compensated at 85% via positive feedback using the EC-Lab software. Solution resistance varied across electrolyte concentrations but was generally between 50−300 Ω.

Controlled-potential electrolysis (CPE) experiments were conducted at room temperature in previously reported custom, gas-tight, two-chamber U-cell.[37] The modified working electrode was held in a RDE internal hardware kit (Pine Research Instrumentation) and mounted into a custom PEEK sleeve. For the electrolysis measurements, the main chamber held the working electrode and an SCE reference electrode in ~ 25 mL electrolyte, and the headspace was measured after each experiment by measuring the amount of ultrapure water needed to refill the main chamber. The auxiliary chamber held the auxiliary carbon rod electrode in 15 mL electrolyte. The two chambers were separated by Nafion membrane. Prior to each experiment, both chambers were sparged with CO_2 for ~20 min, the pH was adjusted, the cell was sparged with CO_2 for ~20 min, and then the main chamber was sealed under CO_2 atmosphere. The pH of the electrolyte was measured immediately prior to the sealing of the cell after CO_2 purge. The resistance of the cell was measured with a single-point high-frequency impedance measurement but was not compensated over the course of the experiment. In general, our electrochemical cell for CPE had Ru ~ 150 Ω in all pH solutions. Unless otherwise noted, CPE experiments were conducted for 2 h.

Product Detection and Quantification

After each CPE experiment, a gaseous sample from the headspace was collected and analyzed using gas chromatography (GC). Analysis was conducted using a Thermo Scientific Trace 1310 GC system with two separate analyzer channels for the detection of H_2 and C1-C2 products. A

Pressure-Lok gas-tight syringe (10 mL, Valco VICI Precision Sampling, Inc.) was used to collect 5 mL aliquots from the main chamber headspace of the cell, and each aliquot was injected directly into the 3 mL sample loop. Using a custom valve system, column configuration, and method provided by Thermo Scientific, gases were separated such that H_2 was detected on the first channel using an Ar carrier gas and thermal conductivity detector (TCD) and all other gases were detected on the second channel using a He carrier gas and a TCD. The GC system was calibrated using calibration gas mixtures (SCOTTY Specialty Gas) at H_2 = 0.02, 0.05, 0.5, and 1% v/v and CO = 0.02, 0.05, 0.5, 1, and 7% v/v. Chromatographs were analyzed by using the Chromeleon Console. Faradaic efficiencies of gaseous products were calculated via Equation 4:

$$\mathrm{FE} = \frac{\frac{V_{HS}}{V_g} \times G \times n \times F}{Q} \tag{4}$$

where V_{HS} is the headspace volume in mL of the working chamber, V_g is the molar volume of gas at 25ºC and 1.0 atm (24500 mL/mol), G is the volume percent of gaseous product determined by GC (%), n is the number of electrons required for each product (n = 2 for H_2 and CO), F is the Faraday constant (C/mol) and Q is the charge passed in Coulombs. Note that the determined Faradaic efficiency values of H_2 and CO accounted for nearly 100% of the charge passed and previous studies under similar aqueous conditions did not yield solution-phase products,[37,42,48] so we did not collect liquid samples for analysis from the working electrode chamber following the CPE experiments.

Ex Situ Infrared Spectroscopy

To evaluate the fractional protonation of P4VP layers by different buffer solutions, *ex situ* transmission infrared experiments were performed using a Nicolet iS50 FTIR with an MCT detector. Each P4VP layer was prepared by drop casting 38.1 μL of a 1% P4VP/DMF solution onto a clean 0.5" diameter uncoated CaF_2 window (Thorlabs, Inc.) and dried in an oven at 60°C overnight to evaporate the DMF. Buffer solutions were prepared and brought to the desired pH as described above. Onto each P4VP-coated window, a 150-μL droplet of buffer solution at the desired pH was deposited and allowed to soak into the polymer coating for 45 minutes. The buffer droplet was then removed via pipette, and any remaining liquid buffer was wicked away using a Kimwipe. The window was dried in an oven at 60°C for 1 hour to evaporate any residual water. To collect spectra (before and after buffer exposure), the windows were mounted inside the FTIR transmission chamber, and backgrounded against a clean CaF_2 window with a dry N_2 purge. Each spectrum was collected with 128 scans at 2 cm^{-1} resolution (data spacing of 0.241 cm^{-1}). Spectra were collected for samples between pH 4 and pH 7—results for pH 3 were unreliable due to optical degradation of the layers.

RESULTS AND DISCUSSION

The Impact of Bulk pH on Fractional Protonation, CO_2RR Selectivity and Activity

We hypothesized that the fractional protonation of the pyridyl moieties could be modeled as a function of pKa of the protonated pyridyl residues and the bulk pH of the electrolyte (Figure 1). While it is challenging to model the exact protonation levels because the pKa of pyridinium in the polymer is difficult to measure accurately, we expected the fractional protonation of the polymer to influence other measurable characteristics of the system (catalytic mechanism, CO_2RR activity,

and reaction selectivity). Specifically, we formed hypotheses that are visualized in Figures b-d. Figure 1b illustrates the postulate that as the bulk pH increased, there would be a decrease in the number of protonated pyridyl residues in the CoPc-P4VP composite, limiting proton delivery to the catalyst active sites. We further hypothesized that this postulated decrease in the fractional protonation of the P4VP would lead to a corresponding increase in reaction selectivity for CO_2RR by CoPc-P4VP over the competing HER (Figure 1c). However, we also hypothesized that as the bulk pH increased, there would be a decrease in CO_2RR activity by CoPc-P4VP composite due to the decreased proton delivery (Figure 1d). Thus, we postulated that CO production by CoPc-P4VP would reach a maximum at intermediate pH ~ 5, where proton availability would be sufficient for the CO_2RR but delivery would be sluggish enough to inhibit competitive HER.

We first used *ex situ* infrared spectroscopy to evaluate the effect of bulk electrolyte solution pH on fractional protonation of the P4VP layer. P4VP exhibits a set of ring-stretching bands in the 1400-1650 cm^{-1} region—analogous to those of pyridine—which are sensitive to protonation of the nitrogen. Previous studies have made band assignments for pyridine,[57] pyridinium,[58,59] neutral P4VP,[60] and protonated P4VP. [61-65] In particular, the 8a ring-stretching band at 1596 cm^{-1} in neutral P4VP shifts to 1637 cm^{-1} when the ring is protonated, providing a convenient indicator of the relative state of protonation in the layer.[59,61-63] Due to the overlapping water absorbance band at 1500-1700 cm^{-1}, we evaluated dry P4VP layers. Our method involved exposing the layer to a droplet of buffer for 45 minutes, giving sufficient time for partitioning of buffer species into the layer. All excess buffer was then removed, leaving only that which had soaked into the layer. The layer was then dried, removing the remaining intercalated water but leaving behind the intercalated ions. The effect of the pH of the electrolyte solution on the P4VP ring-stretching modes is shown in Figure 2. The intensity of the 1637 cm^{-1} band increased and that of the 1596 cm^{-1} band decreased

as the pH of the buffer solution decreased, indicating a greater layer protonation. This trend held across all buffer concentrations tested. We interpret this result to mean that exposure to electrolyte with decreasing pH leads to increased fractional protonation within the polymer. Note that we also observe broad spectral features at ~2300 cm^{-1} and ~2800 cm^{-1} associated with sodium phosphate. These peaks suggest that phosphate is partitioning into the P4VP layer. A representative spectra showing phosphate intercalation for P4VP exposed to pH 5 phosphate buffer at different buffer concentrations is shown in the supplementary information as Supplementary Figure S1. Although the preparation of CoPc-P4VP is different from these *ex situ* IR studies (see Supplementary Table S1 and the Experimental), these measurements provide qualitative support consistent with our hypothesis in Figure 1b that the fractional protonation of the P4VP polymer is modulated by the bulk pH.

An important parameter for determining the optimal pH for performance of this reaction was the electrochemical activity, which was determined by measurement of the steady-state current density under rotation at a specified potential. We had hypothesized that the pKa of the polymer would be important for optimal activity, as the delivery of protons is a key component of the CO_2RR, but with high proton availability, HER would dominate most of the current passed in the system. It was important to consider both the total activity and the activity that went toward CO production, as determined by selectivity measurements (Figure 3, controlled potential electrolysis measurements). The results of this activity study are presented in Figure 4, where we see a maximum total activity at a pH of 5 and a plateau for activity going toward CO production at pH 6 and 7. To determine the dependence of the bulk electrolyte pH and resulting extent of P4VP protonation on the reaction selectivity for the CO_2RR by CoPc-P4VP composites, we determined the Faradaic Efficiency for CO production by the CoPc-P4VP system. Controlled potential

electrolysis (CPE) studies were conducted with CoPc-P4VP films containing graphite powder deposited onto glassy carbon electrodes (CoPc-P4VP/GP/GCE) in 0.4 M phosphate buffers of varying pH. The electrolyte also contained 0.5 M $NaClO_4$ to help maintain constant ionic strength of the electrolyte across the pH range investigated. The amount of CO and H_2 produced were measured using gas chromatography from which Faradaic efficiencies were determined. The average Faradaic efficiencies determined from a series of 2-h CPEs at two potentials, −0.647 vs RHE and −0.707 V vs RHE, are shown in Figure 3. In general, Faradaic efficiency for CO increases as a function of increasing pH at each potential. One key difference is that at the more negative potential of −0.707 V vs RHE, more competitive HER to H_2 is observed in bulk pH 3 electrolytes compared to the same conditions at −0.647 V vs RHE. Overall, these results are consistent with our hypothesis shown in Figure 1d that lower bulk pH and fractional P4VP protonation leads to increased reaction selectivity for the CO_2RR over the competitive HER.

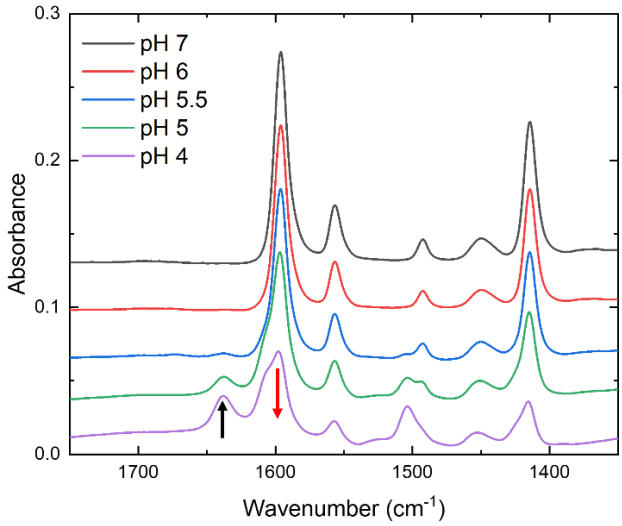

Figure 2. Representative transmission infrared spectra of P4VP layers exposed to 0.2 M sodium phosphate buffer at a range of pH values. The spectra are presented at an offset but without further backgrounding or normalization. The black arrow marks the 1637 cm^{-1} band that rises with decreasing buffer pH, while the red arrow marks the 1596 cm^{-1} band which falls with decreasing buffer pH. Additional ring stretching bands at 1555 cm^{-1}, 1492 cm^{-1}, and 1413 cm^{-1} appear to shift to 1607 cm^{-1},1504 cm^{-1}, and 1423 cm^{-1} respectively in the protonated species. The band at 1450 cm^{-1} arises from CH_2 bending on the P4VP backbone.

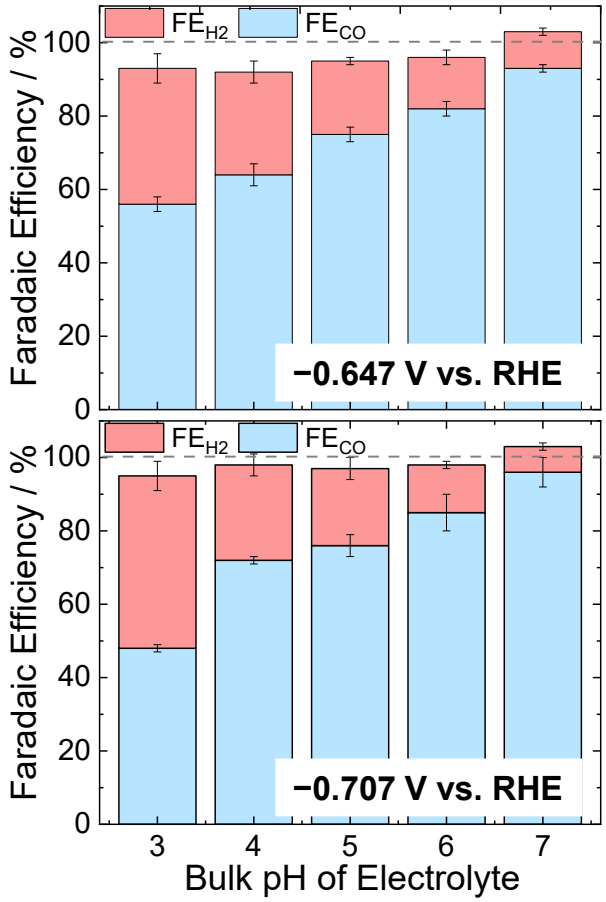

Figure 3. The Faradaic efficiency of the CO_2RR to CO (FE_{CO}) and the HER to H_2 (FE_{H2}) by CoPc-P4VP/GP/GCE in electrolytes with different bulk pH at two different potentials. As the bulk pH increases, there is a corresponding increase in FE_{CO} to a maximum >90% CO production at pH 7. The general trends in FE_{CO} with increasing pH hold are qualitatively similar at −0.647 V vs RHE, the typical potential used for experiments in this manuscript, and at the more negative potential of −0.707 V vs RHE. CPE experiments were performed in a sealed H-cell in 0.4 M phosphate/0.5 M $NaClO_4$ electrolyte as described in the Experimental Section. Data are tabulated in Supplementary Tables S2 and S3, and representative CPE traces are shown in Supplementary Figures S2-S11. All reported Faradaic efficiencies are averages from at least three independent experiments under each condition using identically prepared CoPc-P4VP/GP/GCE electrodes, and the error bars represent standard deviations.

To measure the influence of bulk pH and the resulting fractional protonation of P4VP on the activity of CoPc-P4VP for the CO_2RR, we conducted rotating disk electrode chronoamperometric step (RDE-CA) measurements with CoPc-P4VP/GP/GCE for CO_2 reduction. Here, the RDE electrode is coated with the CoPc-P4VP/GP/GCE composite and then rotated at 1600 rpm to ensure steady-state delivery of CO_2 to the surface of the catalyst-polymer composite film. Representative RDE-CA current traces are shown in Supplementary Figures S12-S16, and the resulting measured average steady-state current densities at −0.647 V vs RHE are summarized in Figure 4 with data tabulated in Supplementary Table S4. In particular, we observe that the magnitude of the total current density ($|j_{total}|$) measured for CoPc-P4VP/GP/GCE in CO_2-saturated electrolyte increases with increasing bulk pH to a maximum at pH 5, and then decreases again at higher pH. However, $|j_{total}|$ takes into account all current density going to both CO production via the CO_2RR and H_2 production via the competitive HER. In Figure 4, we also report the fractional current density going to CO production, $|j_{CO}|$, calculated by correcting $|j_{total}|$ from the RDE-CA measurements with FE_{CO} from the CPE experiments as previously described.[37,48] As shown in Figure 4, $|j_{CO}|$ increases with increasing bulk pH to pH 5 where the activity plateaus at higher pH. These results suggest that the decrease in $|j_{total}|$ at bulk pH > 5 was due to a decrease in HER activity. In contrast, the activity of CoPc-P4VP/GP/GCE for the CO_2RR remains constant at all pH > 5. These results are qualitatively consistent with our postulated activity trends with pH, suggesting that competitive HER inhibits the CO_2RR at CoPc-P4VP/GP/GCE polymer-catalyst composites in CO_2-saturated electrolytes with bulk pH < 5. However, as the pH is increased to pH ≥ 5, the competitive HER is itself inhibited due to low availability of protons as indicated by lower fractional protonation of the P4VP polymer, and CoPc-P4VP/GP/GCE becomes more selective for the CO_2RR.

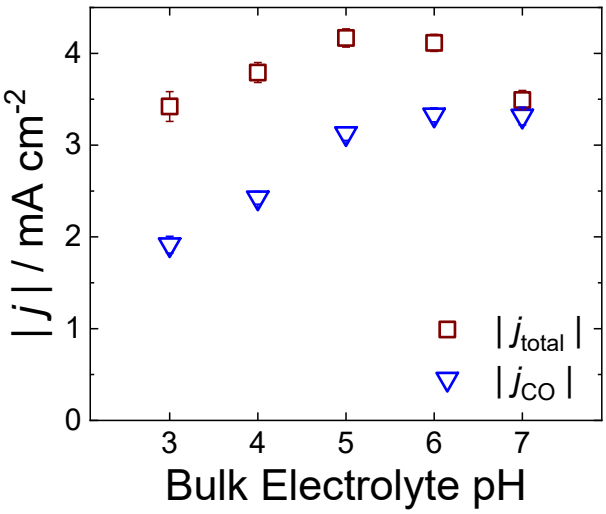

Figure 4. Magnitude of the total current density (j_{total}, red squares) measured for CoPc-P4VP/GP/GCE at −0.647 V vs RHE in CO_2-saturated electrolyte at various pH, and the fractional current density going to CO production (j_{CO}, blue triangles) under the same conditions. The current density measurements were collected from 6-min RDE-CA step experiments at 1600 rpm in electrolytes containing 0.4 M phosphate and 0.5 M $NaClO_4$. Reported j_{total} values are averages from at least three independent experiments under each condition using identically prepared CoPc-P4VP/GP/GCE electrodes, and the error bars represent standard deviations. Reported j_{CO} values were determined from average j_{total} values and average FE_{CO} values, and the error bars represent calculated standard errors. Data are tabulated in Supplementary Table S4, and representative RDE-CA traces can be found in Supplementary Figures S12-S16.

These experimental results are consistent with our hypothesis that increasing the bulk pH decreases the extent of protonation within the polymer, which in turn decreases proton transport to the embedded CoPc sites. This decreased rate of proton transport to the CoPc sites within the polymer inhibits the competitive HER, thereby increasing the reaction selectivity for the CO_2RR. Note that this decreased proton transport could be explained either by a decreased number of multisite proton relays, or by an increase in the local hydrophobicity near the CoPc sites. We do know that proton relays are crucial for CO_2RR, even in hydrophobic environments—previous

studies of the CO_2RR by CoPc embedded in polystyrene polymers with no proton relays showed dramatically decreased activity for the CO_2RR compared to both the CoPc parent system and the CoPc-P4VP.[37,46] However, we cannot fully deconvolute the effect of bulk pH on hydrophobicity or the availability of multisite proton relays. What is clear is that the increased bulk pH alters the local microenvironment near the polymer-embedded CoPc sites, decreasing proton availability for the CO_2RR.

The Impact of Bulk pH on Axial Coordination of P4VP Residues to CoPc

In addition to playing an important role in regulating proton delivery, the pyridyl residues in P4VP also axially coordinate to CoPc to enhance CO_2 binding affinity and overall CO_2RR activity.[37,48] In a previous *in situ* X-ray absorbance spectroscopy (XAS) study, we showed that the pyridyl residues in P4VP coordinated to CoPc in CoPc-P4VP polymer-catalyst composite materials, and that this coordination is mostly maintained when exposed to electrolytes with bulk pH $\geq$ 3.[31] Thus, although our *ex situ* IR studies in Figure 2 indicate that fractional protonation of the P4VP polymer increases as pH decreases, the previous XAS measurements suggest that the local pH near the active site is not sufficiently low to interrupt the coordination between the CoPc and pyridyl residues (e.g. "protonate off" the pyridyl residues). The ability of the polymer residues to axially coordinate to the CoPc even at low pH is likely because the ratio of pyridyl moieties within the polymer matrix to CoPc molecules is ~1300:1, so even if most of the pyridyl residues are protonated, we expect that there will be sufficient unprotonated pyridyl residues to coordinate CoPc within the catalyst-polymer microenvironment at pH $\geq$ 3.

To confirm that axial coordination of CoPc to the pyridyl residues in P4VP is important for enhanced catalytic activity at every pH, we compared the activity of CoPc-P4VP/GP/GCE to that of the same composite prepared with poly-2-vinylpyridine, CoPc-P2VP/GP/GCE. The pyridyl residues in P2VP are sterically prevented from coordinating with CoPc in the polymer-catalyst composites,[37,42] and this has been verified with *in situ* XAS measurements.[49] The average steady state current densities for CoPc-P4VP/GP/GCE and CoPc-P2VP/GP/GCE in CO_2-saturated electrolyte at −0.647 V vs RHE are summarized in Figure 5. In general, the measured $|j_{total}|$ for CoPc-P2VP/GP/GCE ($|j_{P2VP}|$) is always lower than that of CoPc-P4VP/GP/GCE ($|j_{P4VP}|$), but the difference between the two grows larger at higher bulk pH. At higher pH, the CO_2RR becomes the dominant reaction, and axial coordination enhances the activity of this reaction[37,48,49]—hence the larger difference between the current densities measured at higher pH for CoPc-P4VP/GP/GCE and CoPc-P2VP/GP/GCE, for which axial coordination is not possible. Note that the CoPc concentration in CoPc-P2VP/GP/GCE system is slightly higher than that in the CoPc-P4VP/GP/GCE system (Supplementary Table S1). However, the slightly higher catalyst loading in CoPc-P2VP/GP/GCE cannot explain our observed trend that CoPc-P2VP/GP/GCE is less catalytically active for the CO_2RR when compared to CoPc-P4VP/GP/GCE under otherwise equivalent conditions.

We have also shown in previous studies that CoPc-P2VP composites have lower selectivity for CO production compared to CoPc-P4VP.[37,42] In this study, we measured FE_{CO} for CoPc-P2VP/GP/GCE at bulk pH 5, and showed that it operates with $FE_{CO} \sim 58\%$ under these conditions compared to $FE_{CO} \sim 75\%$ for CoPc-P4VP/GP/GCE under analogous conditions (Supplementary Table S5). The results confirm that axial coordination to CoPc is crucial to obtain optimal activity and selectivity in polymer-catalyst composite films, even at different bulk electrolyte pH.[56]

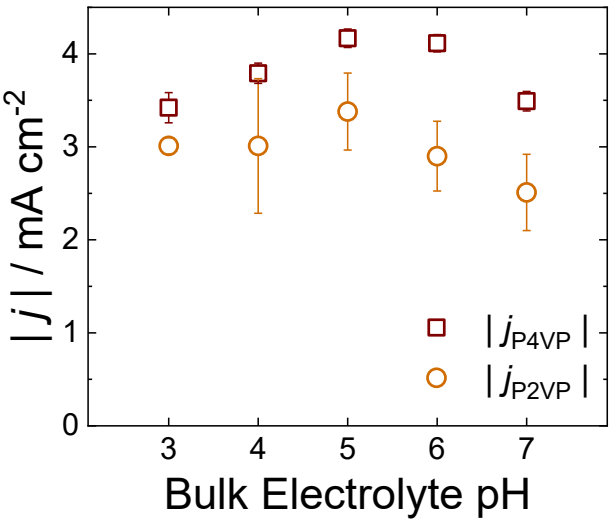

Figure 5. Magnitude of the total current density measured for CoPc-P4VP/GP/GCE ($|j_{P4VP}|$, red squares) and CoPc-P2VP/GP/GCE ($|j_{P2VP}|$, orange circles) at −0.647 V vs RHE in CO_2-saturated electrolyte at various pH. The current density measurements were collected from 6-min RDE-CA step experiments at 1600 rpm in electrolytes containing 0.4 M phosphate and 0.5 M $NaClO_4$. Reported $|j_{P4VP}|$ and $|j_{P4VP}|$ values are averages from at least three independent experiments under each condition using identically prepared electrodes, and the error bars represent standard deviations. Data are tabulated in Supplementary Table S6, and representative RDE-CA traces can be found in Supplementary Figures S12-S16 (CoPc-P4VP/GP/GCE) and Supplementary Figures S17-S21 (CoPc-P2VP/GP/GCE).

The Impact of Electrolyte Concentration on Fractional Protonation and CO_2RR Performance

Previous studies conducted by our group for the CO_2RR at CoPc-P4VP and related systems were typically performed using an electrolyte comprised of 0.1 M NaH_2PO_4 with pH 4.7 after CO_2 sparging.[31,37,42,56,66] These conditions were convenient to study catalyst activity and transport in the CoPc-P4VP system—in particular, pH 4.7 is conveniently one pH unit higher than the

estimated pKa range associated with the protonated pyridyl residues within P4VP,[50] allowing us to probe proton relay effects. However, in the present study, a larger 0.4 M NaH_2PO_4 concentration was necessary to maintain bulk pH 7 after the solution was sparged with CO_2. In addition, 0.5 M $NaClO_4$ was added to the electrolyte in this study to prevent changes in ionic strength as we compared across pH ranges. However, in exploratory studies, we found that this higher concentration of ions within the electrolyte also led to changes in the CO_2RR activity and selectivity of our system compared to previous studies under similar conditions. We decided to explore further the role of concentration on the CO_2RR by the CoPc-P4VP system.

First, we used *ex situ* IR spectroscopy as described above to determine the qualitative extent of protonation of P4VP when exposed to electrolytes with different concentration of phosphate buffer. As shown in Figure 6, there is an increase in the intensity of the protonated P4VP ring-stretching mode at ~1637 cm^{-1}—and a corresponding decrease in intensity of the neutral P4VP mode at 1596 cm^{-1}—as electrolyte concentration increased. This result is consistent with increased protonation of the pyridyl residues in P4VP with increasing NaH_2PO_4 concentration. As an aside, note that if we adjust the pH at the higher phosphate concentrations, we still observe the expected increase in the fractional polymer protonation with decreasing pH (Supplementary Figure S22).

Next, we explored the role of increasing phosphate concentration on reaction selectivity (Figure 7a) and activity (Figure 7b) in CPE experiments. In particular, we show that the Faradaic Efficiency for H_2 production increases slightly with increasing NaH_2PO_4 concentration, from FE_{H2} = 17 ± 2% at 0.1 M NaH_2PO_4 to FE_{H2} = 22 ± 1% at 0.4 M NaH_2PO_4, suggesting that the increased fractional protonation of the polymer at increased NaH_2PO_4 concentration increases the production of H_2. However, the overall activity within the system increases in increasing NaH_2PO_4

concentration, leading to an overall increase in the fraction charge going towards CO production (Q_{CO}).

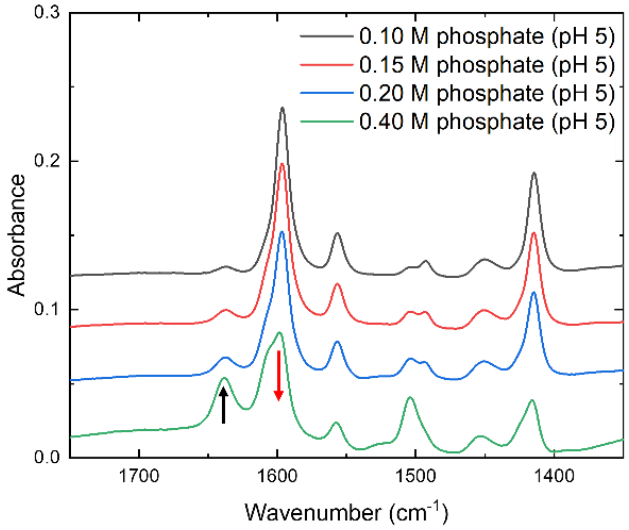

Figure 6. Representative transmission infrared spectra of P4VP layers exposed to pH 5 buffers at a range of electrolyte concentrations. The spectra are presented at an offset but without further backgrounding or normalization. The black arrow marks the 1637 cm^{-1} band that rises with increasing buffer concentration, while the red arrow marks the 1596 cm^{-1} band which falls with decreasing buffer concentration. Additional ring stretching bands at 1555 cm^{-1}, 1492 cm^{-1}, and 1413 cm^{-1} appear to shift to 1607 cm^{-1},1504 cm^{-1}, and 1423 cm^{-1} respectively as buffer concentration increases. The band at 1450 cm^{-1} arises from CH_2 bending on the P4VP backbone.

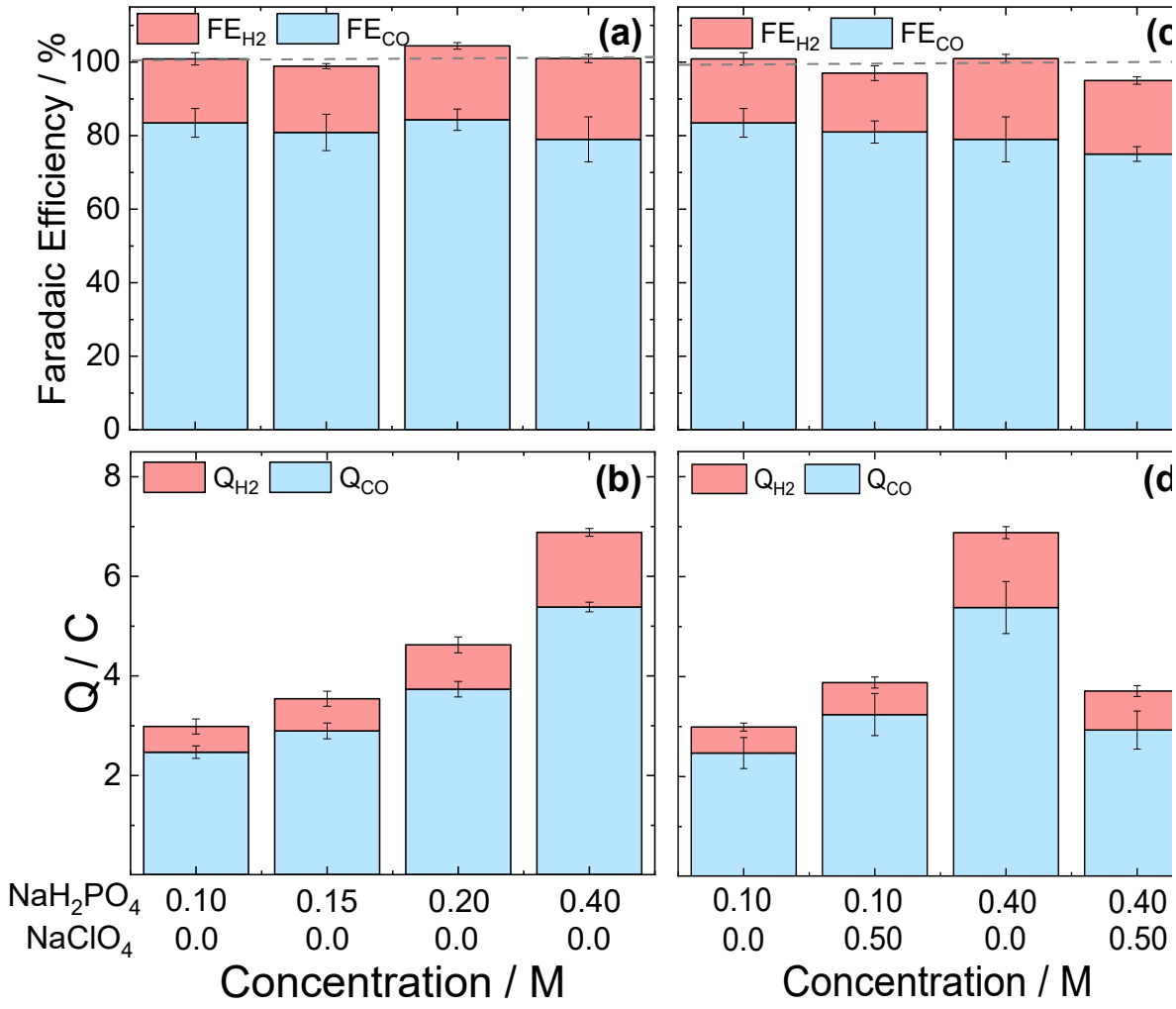

Figure 7. (a) The Faradaic efficiency of the CO_2RR to CO (FE_{CO}) and the HER to H_2 (FE_{H2}) by CoPc-P4VP/GP/GCE in pH 5 electrolytes consisting solely of different concentrations of NaH_2PO_4. (b) The fractional charge going to CO (Q_{CO}) and H_2 (Q_{H2}) from CPE experiments in pH 5 electrolytes consisting solely of different concentrations of NaH_2PO_4. (c) The Faradaic efficiency of the CO_2RR to CO (FE_{CO}) and the HER to H_2 (FE_{H2}) by CoPc-P4VP/GP/GCE in pH 5 electrolytes containing 0.10 M NaH_2PO_4 and 0.40 M NaH_2PO_4 with and without 0.5 M $NaClO_4$. (d) The fractional charge going to CO (Q_{CO}) and H_2 (Q_{H2}) from CPE experiments in in pH 5 electrolytes containing 0.10 M NaH_2PO_4 and 0.40 M NaH_2PO_4 with and without 0.5 M $NaClO_4$. Data are tabulated in Supplementary Tables S7 -S9, representative RDE-CA traces are shown in Supplementary Figures S23-S26, and representative CPE traces are shown in Supplementary Figures S27-S30. Reported Faradaic efficiencies are averages from at least

three independent experiments under each condition using identically prepared CoPc-P4VP/GP/GCE electrodes, and the error bars represent standard deviations. Reported Q_{CO} and Q_{H2} values were determined from average Q values and average FE_{CO} values, and the error bars represent calculated standard errors.

Interestingly, when 0.5 M $NaClO_4$ is added to the system, we do not observe a difference in a Q_{CO} and FE_{CO} with increasing NaH_2PO_4 concentration (Figures 7c-d)—Q_{CO} ~ 4 C and FE_{CO} ~ 82 % regardless of NaH_2PO_4 concentration when 0.5 M $NaClO_4$ is present. *Ex situ* IR spectroscopy of P4VP exposed to solutions containing both 0.1 M NaH_2PO_4 and 0.5 M $NaClO_4$ show a larger increase in the intensity of the protonated P4VP ring-stretching mode at ~1637 cm^{-1}—and a corresponding decrease in intensity of the neutral P4VP mode at 1596 cm^{-1}—compared to P4VP exposed to solutions containing only NaH_2PO_4 (Supplementary Figure S31). This enhancement in the extent of P4VP protonation in NaH_2PO_4 containing $NaClO_4$ is qualitatively similar at both 0.1 M and 0.5 M $NaClO_4$ concentrations (Supplementary Figure S32). Importantly, P4VP exposed to solutions of $NaClO_4$ with no NaH_2PO_4 present show evidence of minimal protonation (Supplementary Figure S33). These results suggest that $NaClO_4$ is not involved in the direct protonation of the pyridyl residues in P4VP, but rather facilitates protonation by NaH_2PO_4 solutions.

It is difficult to deconvolute the interrelated effects of NaH_2PO_4 concentration, ionic strength, and fractional protonation on the CO_2RR activity and selectivity in the CoPc-P4VP/GP/GCE system. The identity and concentration of buffers and electrolytes have complex effects on the catalytic mechanisms and kinetics for the CO_2RR by molecular catalyst species.[67-69] Understanding the complicated nature of the influence of buffer concentration on the CO_2RR in CoPc-P4VP/GP/GCE is made even more difficult by the inclusion of the polymer layer with its own influence over CO_2RR mechanism and kinetics. Nevertheless, a few key insights can be

gained from our studies. First, increasing NaH_2PO_4 concentration in perchlorate-free electrolytes leads to both an increase in the fractional protonation of the P4VP polymer and an increase in catalytic activity for the CO_2RR by the CoPc-P4VP/GP/GCE system. This suggests that the phosphate buffer plays an important role in increasing H^+ partitioning into the P4VP polymer, thus improving H^+ transport to the CoPc active sites. This increased partitioning of H^+ into P4VP at high phosphate buffer concentrations could be due to increased buffer capacity near the polymer/solution interface, or increased partitioning of phosphate buffer anions into the polymer layer to stabilize the positive charge of the protonated pyridinium moieties, effectively "wicking" H^+ into the polymer interior.[70,71]

The CO_2RR performance of CoPc-P4VP/GP/GCE in the presence of 0.5 M $NaClO_4$ and varying NaH_2PO_4 concentrations is more difficult to understand. At the low phosphate buffer concentration of 0.1 M NaH_2PO_4, addition of 0.5 M $NaClO_4$ increases the activity for the CO_2RR from $Q_{CO} = 2.8 \pm 0.8$ C with no $NaClO_4$ present to $Q_{CO} = 4.0 \pm 0.5$ C in 0.5 M $NaClO_4$. However, at the high buffer concentration of 0.4 M NaH_2PO_4, addition of 0.5 M $NaClO_4$ *decreases* the activity for the CO_2RR from $Q_{CO} = 3.9 \pm 0.5$ C with no $NaClO_4$ present to $Q_{CO} = 6.8 \pm 0.4$ C in 0.5 M $NaClO_4$. The increase in activity with added $NaClO_4$ at low phosphate buffer concentration may suggest that anion penetration to stabilize protonated pyridinium residues is important for H^+ partitioning and transport within the CoPc-P4VP polymers, even if the anions are not buffering anions. However, the decrease in activity with increasing $NaClO_4$ concentration at high phosphate concentration may suggest too high of an ionic strength inhibits activity. This inhibition at high ionic strength could be due to a "salting out" effect, where high ionic concentrations within the polymer decrease local CO_2 solubility, and thus decrease CO_2 partitioning and transport.[70,72-74] Although we were able to make a few observations in this manuscript regarding electrolyte

concentration on CO_2RR activity for this polymer-catalyst system, it is clear that the complicated influence of added $NaClO_4$ and NaH_2PO_4 on CO_2RR activity in CoPc-P4VP/GP/GCE will require significant additional studies to understand fully.

CONCLUSIONS

We have presented results showing that the activity and reaction selectivity for the CO_2 reduction reaction (CO_2RR) over the competitive hydrogen evolution reaction (HER) in polymer-catalyst composites is influenced by both bulk electrolyte pH and concentration. In particular, we showed that when CoPc is encapsulated within P4VP polymers and adhered to an electrode surface, the microenvironment of the resulting CoPc-P4VP/GP/GCE can be explicitly modulated by changing a phosphate buffer pH and buffer concentration. Increasing the buffer pH decreases the fractional protonation of pyridyl units within the P4VP polymer as confirmed by *ex situ* IR spectroscopy. This decreased fractional protonation of the P4VP polymer with increased pH leads to a corresponding increase in reaction selectivity for the CO_2RR over the competitive HER, and an increase in the fractional current density going to CO production. Comparisons of electrocatalytic performances by RDE-CA measurements of CoPc-P4VP/GP/GCE and CoPc-P2VP/GP/GCE show higher activity by the former system at every pH investigated. These results suggest that axial coordination of the CoPc to the pyridyl units within the P4VP polymer is crucial to maximize CO_2RR performance. In the case of P2VP, the lower activity observed in this study is consistent with our previous work showing that P2VP polymers are sterically prevented from coordinating with CoPc, resulting in lower activity for the CoPc-P4VP composite films.[37,46]

We also observed an increase in fractional protonation of the P4VP polymer with increasing phosphate buffer concentration, leading to increased activity at higher phosphate concentrations

in pH 5 buffers. This result suggests that increased phosphate buffer concentration leads to increased H^+ partitioning and transport within the P4VP polymer, possibly due to buffering kinetics or increased anion partitioning within the polymer that helps stabilize cationic pyridinium residues and effectively "wicks" H^+ deeper into the polymer-catalyst composite films. However, a more complicated dependence is observed in the non-buffering anion $NaClO_4$ is added to the system—the addition of 0.5 $NaClO_4$ increases CO_2RR activity by CoPc-P4VP/GP/GCE exposed to low 0.1 M phosphate buffer concentrations but decreases CO_2RR activity by the same polymer-catalyst composites exposed to high 0.4 M phosphate buffer concentrations. We postulate that in the lower ionic strength solutions, H^+ transport is further enhanced by the addition of another penetrating anion, ClO_4^-, which can intercalate within the polymer to stabilize cationic pyridinium residues on the P4VP polymer. However, in higher ionic strength solutions, we postulate that the intercalations of anions can effectively "salt out" CO_2, leading to decreased CO_2 solubility and partitioning within the P4VP polymer, and thus decreasing CO_2RR activity.

We believe the studies presented here are informative and provide important insights into how electrolyte influence fractional protonation within protonatable polymers, and how this fractional protonation further influences CO_2RR activity and stability in polymer-catalyst composite films. However, it is clear that more in-depth studies and modeling will be required to understand fully the impact of buffer pH and electrolyte concentration on CO_2RR activity for polymer-catalyst composite films. Additional studies might help deconvolute the effects of the hydrophobicity of the polymer from the microenvironment, and may include kinetic isotope analysis or proton inventory studies to determine changes to the rate-determining step and/or proton relays within the CoPc-P4VP system as a function of pH and electrolyte concentrations. Such studies are ongoing within our group.

ACKNOWLEDGMENTS

This work was supported by an NSF-CAREER grant (CHE 1751791) and a Cottrell Scholar award, a program of the Research Corporation for Science Advancement. T. L. S., W. S. D., and K. E. R. C. were partially supported by the National Science Foundation Graduate Research Fellowship Program (DGE 1256260). T. L. S. acknowledges additional partial support from a University of Michigan Rackham Merit Fellowship. K. E. R. C. acknowledges additional partial support from a Ford Foundation Pre-Doctoral Fellowship, and a National GEM Consortium Fellowship. J.B.E. was partially supported by a Walter Yates Award from the University of Michigan.

ASSOCIATED CONTENT

Supporting Information. Supporting Information is available free of charge on the ACS website. Publications website at DOI: 10.1021/XXX.

- Additional details and tabulated data regarding catalyst and polymer loading and preparation conditions, tabulated activity measurements, tabulated Faradaic efficiencies, representative RDE-CAs, and representative RDE-CPEs.

AUTHOR INFORMATION

Corresponding Author

*Email for C. C. L. M.: cmccrory@umich.edu

Author Contributions

The manuscript was written through contributions of all authors. All authors have given approval to the final version of the manuscript.

ORCID

Taylor L. Soucy: 0000-0002-0090-6721

William S. Dean: 0000-0002-6686-5387

Kevin E. Rivera Cruz: 0000-0001-6690-1571

Jonah B. Eisenberg: 0000-0003-3581-6926

Charles C. L. McCrory: 0000-0001-9039-7192

REFERENCES

(1) Roy, S. C.; Varghese, O. K.; Paulose, M.; Grimes, C. A. "Toward Solar Fuels: Photocatalytic Conversion of Carbon Dioxide to Hydrocarbons," *ACS Nano* **2010**, *4*, 1259-1278. https://dx.doi.org/10.1021/nn9015423

(2) Verma, S.; Kim, B.; Jhong, H.-R. M.; Ma, S.; Kenis, P. J. A. "A Gross-Margin Model for Defining Technoeconomic Benchmarks in the Electroreduction of CO2," *ChemSusChem* **2016**, *9*, 1972-1979. https://dx.doi.org/10.1002/cssc.201600394

(3) Nocera, D. G. "Solar Fuels and Solar Chemicals Industry," *Acc. Chem. Res.* **2017**, *50*, 616-619. https://dx.doi.org/10.1021/acs.accounts.6b00615

(4) Spurgeon, J. M.; Kumar, B. "A comparative technoeconomic analysis of pathways for commercial electrochemical CO2 reduction to liquid products," *Energy Environ. Sci.* **2018**, *11*, 1536-1551. https://dx.doi.org/10.1039/C8EE00097B

(5) Luna, P. D.; Hahn, C.; Higgins, D.; Jaffer, S. A.; Jaramillo, T. F.; Sargent, E. H. "What would it take for renewably powered electrosynthesis to displace petrochemical processes?," *Science* **2019**, *364*, eaav3506. https://dx.doi.org/doi:10.1126/science.aav3506

(6) Crabtree, R. H. "Alternate Strategies for Solar Fuels from Carbon Dioxide," *ACS Energy Lett.* **2020**, *5*, 2505-2507. https://dx.doi.org/10.1021/acsenergylett.0c01359

(7) Mustafa, A.; Lougou, B. G.; Shuai, Y.; Wang, Z.; Tan, H. "Current technology development for CO2 utilization into solar fuels and chemicals: A review," *J. Energy Chem.* **2020**, *49*, 96-123. https://dx.doi.org/10.1016/j.jechem.2020.01.023

(8) Jin, S.; Hao, Z.; Zhang, K.; Yan, Z.; Chen, J. "Advances and Challenges for the Electrochemical Reduction of CO2 to CO: From Fundamentals to Industrialization," *Angew. Chem. Int. Ed.* **2021**, *60*, 20627-20648. https://dx.doi.org/https://doi.org/10.1002/anie.202101818

(9) Park, S.; Wijaya, D. T.; Na, J.; Lee, C. W. "Towards the Large-Scale Electrochemical Reduction of Carbon Dioxide," *Catalysts* **2021**, *11*, 253.

(10) Senftle, T. P.; Carter, E. A. "The Holy Grail: Chemistry Enabling an Economically Viable CO_2 Capture, Utilization, and Storage Strategy," *Acc. Chem. Res.* **2017**, *50*, 472-475. https://dx.doi.org/10.1021/acs.accounts.6b00479

(11) Abe, T.; Imaya, H.; Yoshida, T.; Tokita, S.; Schlettwein, D.; Wöhrle, D.; Kaneko, M. "Electrochemical CO 2 reduction catalysed by cobalt octacyanophthalocyanine and its mechanism," *Journal of Porphyrins and Phthalocyanines* **1997**, *1*, 315-321.

(12) Torbensen, K.; Joulié, D.; Ren, S.; Wang, M.; Salvatore, D.; Berlinguette, C. P.; Robert, M. "Molecular Catalysts Boost the Rate of Electrolytic CO2 Reduction," *ACS Energy Lett.* **2020**, *5*, 1512-1518. https://dx.doi.org/10.1021/acsenergylett.0c00536
(13) Zhang, S.; Fan, Q.; Xia, R.; Meyer, T. J. "CO2 Reduction: From Homogeneous to Heterogeneous Electrocatalysis," *Acc. Chem. Res.* **2020**, *53*, 255-264. https://dx.doi.org/10.1021/acs.accounts.9b00496
(14) Abdinejad, M.; Hossain, M. N.; Kraatz, H.-B. "Homogeneous and heterogeneous molecular catalysts for electrochemical reduction of carbon dioxide," *RSC Advances* **2020**, *10*, 38013-38023. https://dx.doi.org/10.1039/D0RA07973A
(15) Costentin, C.; Robert, M.; Saveant, J. M. "Catalysis of the electrochemical reduction of carbon dioxide," *Chem. Soc. Rev.* **2013**, *42*, 2423-2436. https://dx.doi.org/10.1039/c2cs35360a 10.1039/c2cs35360a. Epub 2012 Dec 11.
(16) Smith, P. T.; Nichols, E. M.; Cao, Z.; Chang, C. J. "Hybrid Catalysts for Artificial Photosynthesis: Merging Approaches from Molecular, Materials, and Biological Catalysis," *Acc. Chem. Res.* **2020**, *53*, 575-587. https://dx.doi.org/10.1021/acs.accounts.9b00619
(17) Costentin, C.; Robert, M.; Savéant, J.-M. "Molecular catalysis of electrochemical reactions," *Curr. Opin. Electrochem.* **2017**, *2*, 26-31. https://dx.doi.org/10.1016/j.coelec.2017.02.006
(18) Sun, L.; Reddu, V.; Fisher, A. C.; Wang, X. "Electrocatalytic reduction of carbon dioxide: opportunities with heterogeneous molecular catalysts," *Energy & Environmental Science* **2020**, *13*, 374-403. https://dx.doi.org/10.1039/C9EE03660A
(19) Nam, D. H.; De Luna, P.; Rosas-Hernandez, A.; Thevenon, A.; Li, F.; Agapie, T.; Peters, J. C.; Shekhah, O.; Eddaoudi, M.; Sargent, E. H. "Molecular enhancement of heterogeneous CO2 reduction," *Nat. Mater.* **2020**, *19*, 266-276. https://dx.doi.org/10.1038/s41563-020-0610-2 10.1038/s41563-020-0610-2. Epub 2020 Feb 25.
(20) Lee, M.-Y.; Park, K. T.; Lee, W.; Lim, H.; Kwon, Y.; Kang, S. "Current achievements and the future direction of electrochemical CO2 reduction: A short review," *Critical Reviews in Environmental Science and Technology* **2020**, *50*, 769-815. https://dx.doi.org/10.1080/10643389.2019.1631991
(21) Long, C.; Li, X.; Guo, J.; Shi, Y.; Liu, S.; Tang, Z. "Electrochemical Reduction of CO2 over Heterogeneous Catalysts in Aqueous Solution: Recent Progress and Perspectives," *Small Methods* **2019**, *3*, 1800369. https://dx.doi.org/https://doi.org/10.1002/smtd.201800369
(22) Ma, T.; Fan, Q.; Tao, H.; Han, Z.; Jia, M.; Gao, Y.; Ma, W.; Sun, Z. "Heterogeneous electrochemical CO2 reduction using nonmetallic carbon-based catalysts: current status and future challenges," *Nanotechnology* **2017**, *28*, 472001. https://dx.doi.org/10.1088/1361-6528/aa8f6f 10.1088/1361-6528/aa8f6f.
(23) Herranz, J.; Pătru, A.; Fabbri, E.; Schmidt, T. J. "Co-electrolysis of CO2 and H2O: From electrode reactions to cell-level development," *Curr. Opin. Electrochem.* **2020**, *23*, 89-95. https://dx.doi.org/https://doi.org/10.1016/j.coelec.2020.05.004
(24) Zheng, T.; Jiang, K.; Wang, H. "Recent Advances in Electrochemical CO2-to-CO Conversion on Heterogeneous Catalysts," *Adv. Mater.* **2018**, *30*, 1802066. https://dx.doi.org/10.1002/adma.201802066
(25) Nitopi, S.; Bertheussen, E.; Scott, S. B.; Liu, X.; Engstfeld, A. K.; Horch, S.; Seger, B.; Stephens, I. E. L.; Chan, K.; Hahn, C.; Nørskov, J. K.; Jaramillo, T. F.; Chorkendorff, I. "Progress and Perspectives of Electrochemical CO2 Reduction on Copper in Aqueous Electrolyte," *Chem. Rev.* **2019**, *119*, 7610-7672. https://dx.doi.org/10.1021/acs.chemrev.8b00705

(26) Kuhl, K. P.; Cave, E. R.; Abram, D. N.; Jaramillo, T. F. "New insights into the electrochemical reduction of carbon dioxide on metallic copper surfaces," *Energy Environ. Sci.* **2012**, *5*, 7050-7059. https://dx.doi.org/10.1039/c2ee21234j
(27) Saha, P.; Amanullah, S.; Dey, A. "Selectivity in Electrochemical CO2 Reduction," *Accounts of Chemical Research* **2022**, *55*, 134-144. https://dx.doi.org/10.1021/acs.accounts.1c00678
(28) Boutin, E.; Wang, M.; Lin, J. C.; Mesnage, M.; Mendoza, D.; Lassalle-Kaiser, B.; Hahn, C.; Jaramillo, T. F.; Robert, M. "Aqueous Electrochemical Reduction of Carbon Dioxide and Carbon Monoxide into Methanol with Cobalt Phthalocyanine," *Angew. Chem. Int. Ed.* **2019**, *58*, 16172-16176. https://dx.doi.org/10.1002/anie.201909257
(29) Rivera Cruz, K. L., Y.; Soucy, T. L.; Zimmerman, P. M.; McCrory, C. "Increasing the CO2 Reduction Activity of Cobalt Phthalocyanine by Modulating the σ-Donor Strength of Axially Coordinating Ligands," *ChemRxiv* **2021**. https://dx.doi.org/https://doi.org/10.26434/chemrxiv.14555841.v2
(30) Soucy, T. L.; Liu, Y.; Eisenberg, J. B.; McCrory, C. C. L. "Enhancing Electrochemical Carbon Dioxide Reduction by Polymer-Encapsulated Cobalt Phthalocyanine through Incorporation of Graphite Powder.," *ChemRxiv* **2021**. https://dx.doi.org/10.33774/chemrxiv-2021-bz00c
(31) Liu, Y.; Deb, A.; Leung, K. Y.; Nie, W.; Dean, W. S.; Penner-Hahn, J. E.; McCrory, C. C. L. "Determining the coordination environment and electronic structure of polymer-encapsulated cobalt phthalocyanine under electrocatalytic CO2 reduction conditions using in situ X-Ray absorption spectroscopy," *Dalton Trans* **2020**, *49*, 16329-16339. https://dx.doi.org/10.1039/d0dt01288b
(32) Zhang, H.; Min, S.; Wang, F.; Zhang, Z. "Immobilizing cobalt phthalocyanine into a porous carbonized wood membrane as a self-supported heterogenous electrode for selective and stable CO2 electroreduction in water," *Dalton Trans.* **2020**, *49*, 15607-15611. https://dx.doi.org/10.1039/D0DT03304A
(33) Lin, L.; Liu, T.; Xiao, J.; Li, H.; Wei, P.; Gao, D.; Nan, B.; Si, R.; Wang, G.; Bao, X. "Enhancing CO2 Electroreduction to Methane with a Cobalt Phthalocyanine and Zinc–Nitrogen–Carbon Tandem Catalyst," *Angew. Chem. Int. Ed.* **2020**, *59*, 22408-22413. https://dx.doi.org/https://doi.org/10.1002/anie.202009191
(34) De Riccardis, A.; Lee, M.; Kazantsev, R. V.; Garza, A. J.; Zeng, G.; Larson, D. M.; Clark, E. L.; Lobaccaro, P.; Burroughs, P. W. W.; Bloise, E.; Ager, J. W.; Bell, A. T.; Head-Gordon, M.; Mele, G.; Toma, F. M. "Heterogenized Pyridine-Substituted Cobalt(II) Phthalocyanine Yields Reduction of CO2 by Tuning the Electron Affinity of the Co Center," *ACS Appl. Mater. Interfaces* **2020**, *12*, 5251-5258. https://dx.doi.org/10.1021/acsami.9b18924
(35) Wu, Y.; Hu, G.; Rooney, C. L.; Brudvig, G. W.; Wang, H. "Heterogeneous Nature of Electrocatalytic CO/CO2 Reduction by Cobalt Phthalocyanines," *ChemSusChem* **2020**, *13*, 6296-6299. https://dx.doi.org/10.1002/cssc.202001396
(36) Xia, Y.; Kashtanov, S.; Yu, P.; Chang, L.-Y.; Feng, K.; Zhong, J.; Guo, J.; Sun, X. "Identification of dual-active sites in cobalt phthalocyanine for electrochemical carbon dioxide reduction," *Nano Energy* **2020**, *67*, 104163. https://dx.doi.org/10.1016/j.nanoen.2019.104163
(37) Liu, Y.; McCrory, C. C. L. "Modulating the mechanism of electrocatalytic CO_2 reduction by cobalt phthalocyanine through polymer coordination and encapsulation," *Nat. Commun.* **2019**, *10*, 1683. https://dx.doi.org/10.1038/s41467-019-09626-8

(38) Wu, Y.; Jiang, Z.; Lu, X.; Liang, Y.; Wang, H. "Domino electroreduction of CO_2 to methanol on a molecular catalyst," *Nature* **2019**, *575*, 639-642. https://dx.doi.org/10.1038/s41586-019-1760-8
(39) Zhu, M.; Chen, J.; Guo, R.; Xu, J.; Fang, X.; Han, Y.-F. "Cobalt phthalocyanine coordinated to pyridine-functionalized carbon nanotubes with enhanced CO2 electroreduction," *Appl. Catal. B* **2019**, *251*, 112-118. https://dx.doi.org/10.1016/j.apcatb.2019.03.047
(40) Lieber, C. M.; Lewis, N. S. "Catalytic reduction of carbon dioxide at carbon electrodes modified with cobalt phthalocyanine," *J. Am. Chem. Soc.* **1984**, *106*, 5033-5034. https://dx.doi.org/10.1021/ja00329a082
(41) Meshitsuka, S.; Ichikawa, M.; Tamaru, K. "Electrocatalysis by metal phthalocyanines in the reduction of carbon dioxide," *Journal of the Chemical Society, Chemical Communications* **1974**, 158-159. https://dx.doi.org/10.1039/C39740000158
(42) Kramer, W. W.; McCrory, C. C. L. "Polymer coordination promotes selective CO_2 reduction by cobalt phthalocyanine," *Chem. Sci.* **2016**, *7*, 2506-2515. https://dx.doi.org/10.1039/C5SC04015A
(43) Abe, T.; Yoshida, T.; Tokita, S.; Taguchi, F.; Imaya, H.; Kaneko, M. "Factors affecting selective electrocatalytic co2 reduction with cobalt phthalocyanine incorporated in a polyvinylpyridine membrane coated on a graphite electrode," *Journal of Electroanalytical Chemistry* **1996**, *412*, 125-132. https://dx.doi.org/https://doi.org/10.1016/0022-0728(96)04631-1
(44) Yoshida, T.; Kamato, K.; Tsukamoto, M.; Iida, T.; Schlettwein, D.; Wöhrle, D.; Kaneko, M. "Selective electroacatalysis for CO_2 reduction in the aqueous phase using cobalt phthalocyanine/poly-4-vinylpyridine modified electrodes," *J. Electroanal. Chem.* **1995**, *385*, 209-225. https://dx.doi.org/10.1016/0022-0728(94)03762-R
(45) Soucy, T. L.; Dean, W. S.; Zhou, J.; Rivera Cruz, K. E.; McCrory, C. C. L. "Considering the Influence of Polymer–Catalyst Interactions on the Chemical Microenvironment of Electrocatalysts for the CO2 Reduction Reaction," *Acc. Chem. Res.* **2022**, *55*, 252-261. https://dx.doi.org/10.1021/acs.accounts.1c00633
(46) Soucy, T. L.; Liu, Y.; Eisenberg, J. B.; McCrory, C. C. L. "Enhancing the Electrochemical CO2 Reduction Activity of Polymer-Encapsulated Cobalt Phthalocyanine Films by Modulating the Loading of Catalysts, Polymers, and Carbon Supports," *ACS Appl. Energy Mater.* **2022**, *5*, 159-169. https://dx.doi.org/10.1021/acsaem.1c02689
(47) Nie, W.; McCrory, C. C. L. "Strategies for breaking molecular scaling relationships for the electrochemical CO2 reduction reaction," *Dalton Trans.* **2022**, *51*, 6993-7010. https://dx.doi.org/10.1039/D2DT00333C
(48) Rivera Cruz, K. E.; Liu, Y.; Soucy, T. L.; Zimmerman, P. M.; McCrory, C. C. L. "Increasing the CO2 Reduction Activity of Cobalt Phthalocyanine by Modulating the σ-Donor Strength of Axially Coordinating Ligands," *ACS Catal.* **2021**, *11*, 13203-13216. https://dx.doi.org/10.1021/acscatal.1c02379
(49) Liu, Y.; Deb, A.; Leung, K. Y.; Nie, W.; Dean, W. S.; Penner-Hahn, J. E.; McCrory, C. C. L. "Determining the coordination environment and electronic structure of polymer-encapsulated cobalt phthalocyanine under electrocatalytic CO_2 reduction conditions using in situ X-Ray absorption spectroscopy," *Dalton Trans.* **2020**, *49*, 16329-16339. https://dx.doi.org/10.1039/D0DT01288B
(50) Kirsh, Y. E.; Komarova, O. P. "Protonization in aqueous solutions of poly-4-vinylpyridine and poly-2-vinylpyridine partially quaternized with dimethyl sulphate," *Polymer Science U.S.S.R.* **1976**, *18*, 223-228. https://dx.doi.org/https://doi.org/10.1016/0032-3950(76)90078-2

(51) Zhang, Z.; Melo, L.; Jansonius, R. P.; Habibzadeh, F.; Grant, E. R.; Berlinguette, C. P. "pH Matters When Reducing CO2 in an Electrochemical Flow Cell," *ACS Energy Lett.* **2020**, *5*, 3101-3107. https://dx.doi.org/10.1021/acsenergylett.0c01606
(52) Henckel, D. A.; Counihan, M. J.; Holmes, H. E.; Chen, X.; Nwabara, U. O.; Verma, S.; Rodríguez-López, J.; Kenis, P. J. A.; Gewirth, A. A. "Potential Dependence of the Local pH in a CO2 Reduction Electrolyzer," *ACS Catal.* **2020**, *11*, 255-263. https://dx.doi.org/10.1021/acscatal.0c04297
(53) Lu, X.; Zhu, C.; Wu, Z.; Xuan, J.; Francisco, J. S.; Wang, H. "In Situ Observation of the pH Gradient near the Gas Diffusion Electrode of CO2 Reduction in Alkaline Electrolyte," *Journal of the American Chemical Society* **2020**, *142*, 15438-15444. https://dx.doi.org/10.1021/jacs.0c06779
(54) Green, A. A. "The Preparation of Acetate and Phosphate Buffer Solutions of Known PH and Ionic Strength," *J. Am. Chem. Soc.* **1933**, *55*, 2331-2336. https://dx.doi.org/10.1021/ja01333a018
(55) Zhong, H.; Fujii, K.; Nakano, Y.; Jin, F. "Effect of CO2 Bubbling into Aqueous Solutions Used for Electrochemical Reduction of CO2 for Energy Conversion and Storage," *J. Phys. Chem. C* **2015**, *119*, 55-61. https://dx.doi.org/10.1021/jp509043h
(56) Soucy, T. L.; Liu, Y.; Eisenberg, J. B.; McCrory, C. C. L. "Enhancing the Electrochemical CO2 Reduction Activity of Polymer-Encapsulated Cobalt Phthalocyanine Films by Modulating the Loading of Catalysts, Polymers, and Carbon Supports," *ACS Applied Energy Materials* **2021**. https://dx.doi.org/10.1021/acsaem.1c02689
(57) Wong, K. N.; Colson, S. D. "The FT-IR spectra of pyridine and pyridine-d5," *J. Mol. Spectrosc.* **1984**, *104*, 129-151. https://dx.doi.org/https://doi.org/10.1016/0022-2852(84)90250-9
(58) Barrow, G. M. "The Nature of Hydrogen Bonded Ion-Pairs: The Reaction of Pyridine and Carboxylic Acids in Chloroform," *J. Am. Chem. Soc.* **1956**, *78*, 5802-5806. https://dx.doi.org/10.1021/ja01603a022
(59) Cook, D. "VIBRATIONAL SPECTRA OF PYRIDINIUM SALTS," *Can. J. Chem.* **1961**, *39*, 2009-2024. https://dx.doi.org/10.1139/v61-271
(60) Atvars, T. D. Z.; Dibbern, D. N.; Sabadini, E. "Infrared Spectroscope And Conformational Analysis Of Poly(4-Vinyl Pyridine) and Its Model Compounds," *Spectrosc. Lett.* **1987**, *20*, 1-15. https://dx.doi.org/10.1080/00387018708082271
(61) Panov, V. P.; Vorontsov, E. D.; Evdakov, V. P. "Spectroscopic determination of the extent of protonation and alkylation of poly-4-vinylpyridine derivatives," *J. Appl. Spectrosc.* **1975**, *23*, 958-962. https://dx.doi.org/10.1007/BF00608822
(62) Smith, P.; Eisenberg, A. "Infrared spectroscopic study of blends of poly(styrene-co-styrenesulfonic acid) with poly(styrene-co-(4-vinylpyridine))," *Macromolecules* **1994**, *27*, 545-552. https://dx.doi.org/10.1021/ma00080a032
(63) Chen, W.; Sauer, J. A.; Hara, M. "The effect of ionic cross-links on the deformation behavior of homoblends made of poly(styrene-co-styrenesulfonic acid) and poly(styrene-co-4-vinylpyridine)," *Polymer* **2003**, *44*, 7729-7738. https://dx.doi.org/https://doi.org/10.1016/j.polymer.2003.09.053
(64) Sakurai, K.; Douglas, E. P.; MacKnight, W. J. "Spectroscopic study of an ionic blend made from the acid form of sulfonated polystyrene and poly[ethyl acrylate-co-(4-vinylpyridine)]," *Macromolecules* **1992**, *25*, 4506-4510. https://dx.doi.org/10.1021/ma00044a008
(65) Qin, S.; Qin, D.; Ford, W. T.; Herrera, J. E.; Resasco, D. E. "Grafting of Poly(4-vinylpyridine) to Single-Walled Carbon Nanotubes and Assembly of Multilayer Films," *Macromolecules* **2004**, *37*, 9963-9967. https://dx.doi.org/10.1021/ma048692p

(66) Rivera Cruz, K. E.; Liu, Y.; Soucy, T. L.; Zimmerman, P. M.; McCrory, C. C. L. "Increasing the CO2 Reduction Activity of Cobalt Phthalocyanine by Modulating the σ-Donor Strength of Axially Coordinating Ligands," *ACS Catalysis* **2021**, 13203-13216. https://dx.doi.org/10.1021/acscatal.1c02379
(67) Zeng, J. S.; Corbin, N.; Williams, K.; Manthiram, K. "Kinetic Analysis on the Role of Bicarbonate in Carbon Dioxide Electroreduction at Immobilized Cobalt Phthalocyanine," *ACS Catal.* **2020**, *10*, 4326-4336. https://dx.doi.org/10.1021/acscatal.9b05272
(68) Schneider, C. R.; Lewis, L. C.; Shafaat, H. S. "The good, the neutral, and the positive: buffer identity impacts CO2 reduction activity by nickel(ii) cyclam," *Dalton Trans.* **2019**, *48*, 15810-15821. https://dx.doi.org/10.1039/C9DT03114F
(69) Carucci, C.; Salis, A.; Magner, E. "Electrolyte effects on enzyme electrochemistry," *Current Opinion in Electrochemistry* **2017**, *5*, 158-164. https://dx.doi.org/https://doi.org/10.1016/j.coelec.2017.08.011
(70) Moghaddam, S. Z.; Thormann, E. "The Hofmeister series: Specific ion effects in aqueous polymer solutions," *J Colloid Interface Sci* **2019**, *555*, 615-635. https://dx.doi.org/10.1016/j.jcis.2019.07.067
(71) Ritt, C. L.; Liu, M.; Pham, T. A.; Epsztein, R.; Kulik, H. J.; Elimelech, M. "Machine learning reveals key ion selectivity mechanisms in polymeric membranes with subnanometer pores," *Science Advances*, *8*, eabl5771. https://dx.doi.org/10.1126/sciadv.abl5771
(72) Hashiba, H.; Weng, L.-C.; Chen, Y.; Sato, H. K.; Yotsuhashi, S.; Xiang, C.; Weber, A. Z. "Effects of Electrolyte Buffer Capacity on Surface Reactant Species and the Reaction Rate of CO2 in Electrochemical CO2 Reduction," *J. Phys. Chem. C* **2018**, *122*, 3719-3726. https://dx.doi.org/10.1021/acs.jpcc.7b11316
(73) Wanderley, R. R.; Evjen, S.; Pinto, D. D. D.; Knuutila, H. K. "The salting-out effect in some physical absorbents for CO2 capture," **2018**.
(74) Okur, H. I.; Hladílková, J.; Rembert, K. B.; Cho, Y.; Heyda, J.; Dzubiella, J.; Cremer, P. S.; Jungwirth, P. "Beyond the Hofmeister Series: Ion-Specific Effects on Proteins and Their Biological Functions," *The Journal of Physical Chemistry B* **2017**, *121*, 1997-2014. https://dx.doi.org/10.1021/acs.jpcb.6b10797

TOC Image: